Journal of Colloid and Interface Science 532 (2018) 171–181

Contents lists available at ScienceDirect

Journal of Colloid and Interface Science

journal homepage: www.elsevier.com/locate/jcis

Regular Article

Nanopatterned protein-polysaccharide thin films by humidity regulated phase separation

Russell A. Banta [a,b,c], Timothy W. Collins [a,b,c], Rickey A. Curley [a,b,c], Paul W. Young [b,d], Justin D. Holmes [a,b,c], Eoin J. Flynn [a,b,c,*]

[a] School of Chemistry, University College Cork, Cork, Ireland
[b] Environmental Research Institute, Lee Road, University College Cork, Cork, Ireland
[c] AMBER@CRANN, Trinity College Dublin, Dublin 2, Ireland
[d] School of Biochemistry and Cell Biology, University College Cork, Ireland

GRAPHICAL ABSTRACT

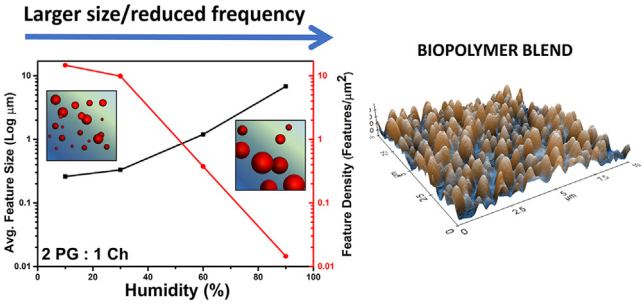

ARTICLE INFO

Article history:
Received 10 March 2018
Revised 20 July 2018
Accepted 24 July 2018
Available online 25 July 2018

Keywords:
Protein
Polysaccharide
Biopolymer
Patterning
Morphology
Phase separation
Ostwald ripening

ABSTRACT

Greater sustainability in mass manufacturing is essential to alleviating anthropogenic climate change. High surface-area, micro- and nano-patterned films have become a fundamental tool in materials science, however these technologies are subject to a dwindling petrochemical supply, increasing costs and disposability concerns. This paper describes the production of patterned biopolymer films utilizing controlled phase separation of biopolymeric thin films into nanopatterns using easily transferable variables and methods. Similar morphologies to those commonly observed with synthetic block-copolymers (BCPs) were achieved across a large range of feature sizes, from 160 nm to >5 μm: Bicontinuous, porous, droplet-matrix, particulated and dimpled. Protein and polysaccharide type, protein to polysaccharide ratio, casting method and ambient humidity were primary conditions found to influence the pore morphology of the films. High protein concentrations (4:1 and 2:1 blends) generally resulted in porous structures whereas high polysaccharide concentrations (1:2 and 1:4 blends) resulted in spherical structures. High humidity conditions (60% + relative humidity) resulted in the growth of large protuberances up to 10 μm in diameter while lower humidity (10–30%) resulted in discrete features smaller than 200 nm.

© 2018 Elsevier Inc. All rights reserved.

1. Introduction

Sustainable materials is a term that encompasses a sustainable, materials science based approach to technological development

* Corresponding author at: Environmental Research Institute, Lee Road, University College Cork, Cork, Ireland.
E-mail address: eoin.flynn@ucc.ie (E.J. Flynn).

https://doi.org/10.1016/j.jcis.2018.07.109
0021-9797/© 2018 Elsevier Inc. All rights reserved.

and product lifecycles. It focusses on bottom-up production methods; biodegradable, renewably sourced materials; and environmentally benign usage. The development of technologies from sustainable sources is essential to minimising negative anthropogenic effects on environment and climate. Resource finitude; waste management; and production and usage emissions need to be addressed. Our most crucial technologies must be prioritised for the initial developments of these new, sustainable materials.

Electronic and smart devices, and advanced medical materials; these are among our most vital modern technologies. High surface-area, micro- and nano-patterned films are fundamental to the manufacture and function of the aforementioned technologies, as well as finding widespread use in a variety of other applications. Apart from semiconductor [1] and medical tech [2], they are critical to superhydrophobic [3], anti-reflective [4,5] and self-cleaning materials [5]; anti-fouling coatings; and food texture technologies [6] (which will be of increasing importance as more and more synthetic food equivalents are required to replace environmentally unsustainable foodstuffs) [7]. The patterns are produced through phase separation of highly refined, synthetic, block-copolymer thin-films [8]. These polymers are a perfect example of a long term, unsustainable material. Sourced from petrochemicals, they will become prohibitively expensive with time, they are non-renewable, non-biodegradable, and the refinement processes of their production are environmentally damaging. Our research shows the development of a sustainable materials alternative; bottom-up production of patterned films from renewable, biodegradable biopolymers.

Biopolymers (proteins and polysaccharides primarily) are an ideal sustainable material, and an obvious alternative to conventional, petrochemical polymers in all but the most specialised applications [9]. They are abundant, readily accessible, renewable, compostable and; produced and extracted with minimal to no environmental impact [10]. Biopolymers also have suite of attractive features for manufacturers; high structural specificity; well-defined and varied functionalities; structure dependant solubility [11]; predictable viscosity [12]; bactericidal properties [13]; and biocompatibility [14]. Molecular weight distributions of polysaccharides can vary [15] but are readily refined [16] and in the case of proteins, monodisperse molecular weight distribution is an innate property. For all the above reasons, naturally occurring biopolymers have interested scientists and engineers for decades. They are used in food texturing [17], personal care products [18], cell binding [19], textiles [20] and membranes [21–23]. Many of these applications involve patterning of biopolymer surfaces; though the structures obtained have so far been much larger than those required for use in applications such as substrate patterning [24–29]. There are only a few notable examples of biopolymer blends being used to create surfaces with structures on a scale akin to those in this work [30–32]. However, these typically involve secondary etch steps, with harsh solvents and functionalised biopolymers to achieve desired morphologies, making them environmentally damaging.

Microphase separation phenomena in biopolymer-biopolymer-solvent systems falls into two categories; associative and segregative [33,34]. Categorisation is dependent on the affinity between the biopolymers and the solvent. Associative phase separation occurs when the biopolymers carry opposite charges, and segregative when they carry the same charge. Complexities arise in the form of; kinetic competition between gelation processes and phase separation process [35]; the influence of shear forces on formation mechanisms [36,37]; the influence of humidity on solution behaviours [38]; and the vagaries of biopolymer structure in solution, to name only a few. This paper reports phase separations of a specific type of biopolymer-biopolymer-solvent system; protein-polysaccharide-solvent solutions (hereafter referred to as the Pr-Ps-S solutions). These solutions are used to produce surface patterned, composite thin-films of polysaccharide and protein. Associative and segregative phase separations of such solutions have been studied extensively over the past four decades, primarily in food science. However, latter work has focussed on limited applications in packaging and biomedical devices [14,17,39,40].

Most scientific literature details phase separation of a variety of proteins and polysaccharides, generally in one type of solvent; water [33,41–44]. The exception is when the polysaccharide of choice is chitosan, when the solvent of choice is typically dilute acetic acid [45–47]. The research reported here builds upon state-of-the-art in the field of biopolymer phase separation in four ways: firstly, unique Pr-Ps-S solutions are studied; proteins are bovine serum albumin (BSA) and pigskin gelatin (PG), polysaccharide is chitosan (Ch), and solvent is formic acid (FA). Secondly, the production of thin-films from these Pr-Ps-S systems is examined with a view to their use in materials applications beyond the food, packaging and biomed industries. Specifically, utilising micro- and nanopatterns in templating, and smart textiles applications. Thirdly, the control of formation conditions under which these phase separations occur is different. Control of conditions such as humidity and ambient temperature is usually more associated with the formation processes of synthetic polymer solutions for medical device and advanced membrane applications [48–51]. Control of biopolymer phase separation of the Pr-Ps-S solutions confers a degree of control over the morphology final thin-films, affecting utility. Fourthly, the analytical data concerning the growth of surface features of the biopolymer thin-films is compared to that of Ostwald ripened structures. The findings described in this paper shows that controlled phase separation of biopolymer blends is an effective method of producing micro- and nano-patterned surfaces.

2. Experimental

2.1. Biopolymers, casting solutions and substrate

Low molecular weight chitosan (50–190 kDa) > 75% deacetylation, high bloom gelatin from porcine skin (~300 bloom, Type A premium grade) and Bovine Serum Albumin (lyophilised powder, ≥96%, molecular weight ~66 kDa) were purchased from Sigma Aldrich. Substrates used in all cases were Fisherbrand™ Microscopic Slides with Ground Edges (plain). The solvent used was Formic acid, 98+ %, pure, ACROS Organics™ and was diluted to 90% w/v before use using distilled water. Casting solutions were prepared using 90% formic acid as solvent to ensure that the biopolymers above were below their isoelectric point in solution and so, positively charged. This was to ensure that any phase separation processes occurring in the Pr-Ps-S solutions were segregative.

2.2. Solution preparation

Prior to dissolution, proteins and polysaccharides were dried overnight at room temperature under vacuum. Polymer stock solutions were made by solubilising chitosan (Ch), bovine serum albumin (BSA) and pigskin Gelatin (PG) in 90% formic acid (FA) acid at 5 w/v% 10 w/v% and 10 w/v%. These solutions were stirred in a closed vessel for 3 hr in a closed container at room temperature. The solutions were then centrifuged at 13,000 rpm in a Beckman Coulter Avanti J-26XPI centrifuge at 18 °C for 15 min and decanted. Following this, stock solutions were stored at −20 °C for further use or used immediately. Stock solutions were diluted with fresh formic acid and/or mixed with each other to produce coating solutions.

2.3. Coating preparation

2.3.1. Thin-film casting

Thin-films were prepared in triplicate using an automatic film applicator, (K202 Control Coater, RK Printcoat Instruments Ltd, UK) to produce biopolymer solution coatings of uniform thickness. Standard conditions: applicator electrical drive speed 3, 12 μm casting bar calibrated to height of thin film substrate (note that initial solution casting thickness does not match final thin-film thickness). Substrates were glass slides onto which single biopolymer solutions and Pr-Ps-S solutions were cast. Humidity controlled experiments were conducted in a purpose built chamber, also described by Idris et al. [52] Air passed through a humidification system. Ambient air was mixed with dry, synthetic air to influence humidity. Humidity control was achieved by passing the air through a Dreschel bottle containing distilled water and air, respectively. Monitoring of humidity was achieved through use of a humidity meter (*HOBO MX Temp/RH Logger*), which also functioned as an ambient temperature meter. Temperature was stabilised by laboratory air conditioning, at approx. 18 °C. Air pressure was normal atmospheric pressure at sea level in our geographical region (approx.10.1 N/cm^2).

2.3.2. Atomic force microscopy (AFM)

The surface topography and phase of the prepared samples was analysed by atomic force microscopy (AFM) using a Park Systems, XE-100 instrument under ambient conditions. Scans were performed in non-contact mode with high resolution, silicon microcantilever tips. Topographic images were recorded at a resonance frequency of 270–300 kHz. Images were analysed using "Gwyddion" and "Park XEI" image analysis software. Features were measured using "Gwyddion" and descriptive statistics calculated using "Origin". Surface roughness was measured using "XEI" software. RMS (*root means square arithmetical mean roughness* or *root means square average roughness*) is the average between the height deviations and the mean line/surface, taken over the evaluation length/area. All figures were calculated from AFM data with equations defined by the Japanese Standards Association [53,54]. Surface feature diameters were measured using the Gwyddion watershed algorithm for scanning probe microscopy. Force-distance mapping was performed using a Park XE-100 AFM using silicon probes (NCSTR, resonance frequency ≈160 kHz, spring constant 7.4 N m^{-1}, tip radius 8 nm). Data was processed using XEI and SPIP software, where young's modulus was calculated using a Hertzian model. A minimum of 64 data points were recorded for each sample.

3. Results and discussion

3.1. Single polymer solution thin-films

Biopolymer thin-films were cast from the three single biopolymers; Ch, BSA and PG. Solutions of 4 w/v%, 2 w/v% and 1 w/v% were used for each, to confirm that no patterned structures were forming from the pure polymers. If present in pure biopolymer films, such features in the composite films would be difficult to distinguish from those due solely to the composite formation mechanisms. Furthermore, their formation may influence the formation of the composite film features. AFM images (see Figure 1 in Supporting Information) showed that films were indistinguishable from one another. No structures likely to align at the interface of the biopolymer domains, thereby increasing mutual solubility of the biopolymers and retarding the phase separation processes of the Pr-Ps-S solutions, were noted.

Supplementary data associated with this article can be found, in the online version, at https://doi.org/10.1016/j.jcis.2018.07.109.

3.2. Pr-Ps-S solution thin-films

3.2.1. Thin-films from phase separation of BSA-Ch-FA solutions

Growth mechanisms typically describe the increase in size of features in phase separated films. This is most typically shown in graphs of feature size per unit time, where, for example, feature diameter is seen to increase with time. Fig. 1 shows AFM images of BSA-Ch composite thin-films cast from BSA-Ch-FA Pr-Ps-S solutions. At biopolymer ratio of 4 w/v% BSA to 1 w/v% Ch, across all humidities (Fig. 1, Column A), predominantly pores were formed. AFM data showed that as the humidity increased, the number of pores increased (Fig. 2a), and the mean pore radius decreased (Fig. 2b); highlighting an inverse correlation between pore growth and humidity. Thus, pore formation at this biopolymer ratio does not occur via a growth mechanism, *i.e.* with an increase of pore mean diameter with time. This is reflected in the negative slope of the trend line for feature size at the 4:1 biopolymer ratio in Fig. 2a in contrast to a positive slope for the other biopolymer ratios (all of which exhibited protuberances as the analysed features). Similarly, in Fig. 2b, the pores show a positive trend to their frequency, *i.e.* increasing frequency, in contrast to the negative trend-line slopes of the protuberances observed at all other biopolymer ratios [51].

At a biopolymer ratio of 2 w/v% BSA to 1 w/v% Ch, (Fig. 1, column B) at 10% and 30% humidity, discontinuous porous domains and protuberances were observed. At 60% and 90% humidity however, (B3 and B4 respectively) no pores were visible and protuberances were solely present, but more globular and larger than those in the images of columns C and D of Fig. 1. The ovoid shape of these protuberances is most likely an attempt at the adoption of a spherical shape, resulting from coalescence. As the only parameter varying in column B is humidity, the large globules observed must result from high humidity conditions. High humidity, *i.e.* 60% +, generates thermodynamic instability in the system which drives phase separation. Excessively high humidity during film formation may excessively increase the water content of the cast solution to be phase separated. This decreases the solubility of any hydrophobic biopolymers in solution; in this instance, Ch [55,56]. This difficult to control reduction in the solubility of Ch within the overall biopolymer solution results in an instability that causes the Ch to crash out. BSA, by contrast is more soluble in formic acid than Ch [57–59]. However, one would expect this effect to be more exaggerated at higher Ch ratios and this does not appear to be the case in the images of Fig. 1, columns C and D.

Across all humidity values, the protuberances follow the general trend outlined above; increasing mean diameter with increasing humidity (Fig. 2a). The aforementioned large jump in the scale of the protuberances results in the slope of the trend line for the data at 2:1 biopolymer ratio in Fig. 2a being the steepest of the four ratios tested. At biopolymer ratio of 1 w/v% BSA to 2 w/v% Ch, across all humidity values (Fig. 1, Column C), only protuberances were formed. Increased humidity resulted in the subsumption of smaller protuberances and interconnects to form much larger well-defined protuberances. This typifies the behaviour of the phase separation of colloidal systems; a growth process proceeding by the nucleation and growth of the dispersed phase from the dispersion medium [60,61]. AFM data in shown in Fig. 2a and b corroborate that the mean density of features decreases and mean feature diameter increases as a function of humidity at this biopolymer ratio. There is one deviation from the trend. In proceeding from 60% to 90% humidity, the feature density decreased while the mean feature diameter increased, also apparent from the AFM images. This is likely due to the increased height of protuberances formed in the 90% blend.

Similar structures to those in shown in image C1 of Fig. 1 (and again in image C1 of Fig. 3 at the same ratio for PG:Ch) were

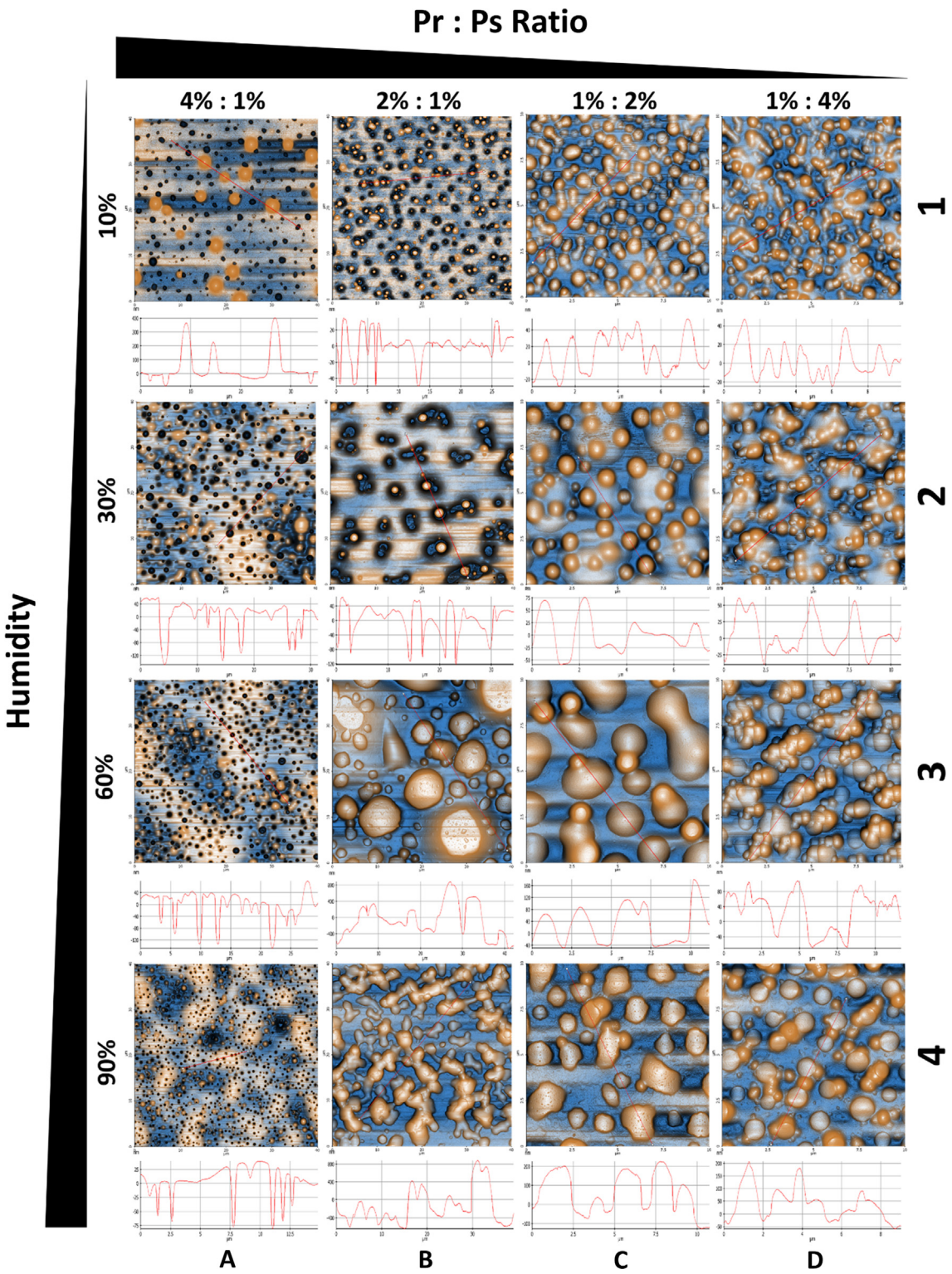

Fig. 1. AFM image grid and associated line profiles showing results of casting thin-films at 12 μm from specific Pr-Ps-S solutions of BSA-Ch-FA at specific humidities. Each image in column A and column B is 40 μm × 40 μm area. Each image in column C and column D is 10 μm × 10 μm area. Column A = 4 w/v% BSA 1 w/v% Ch (4:1), column B = 2 w/v% BSA 1 w/v% Ch (2:1), column C = 1 w/v% BSA 2 w/v% Ch (1:2), column D = 1 w/v% BSA 4 w/v% Ch (1:4). Row 1 = 10% humidity, row 3 = 30% humidity, row 3 = 60% humidity and row 4 = 90% humidity.

observed by de Jong and van de Velde by AFM (their images were of 160 μm × 160 μm area, compared to 10 μm × 10 μm areas here) [35]. In a later publication, the same authors attributed the formation of these structures to nucleation and growth processes in phase separations [62]. They did not specify any particular growth processes. The diameters of the protuberances in the de Jong and van de Velde images are approx. 7–15 μm, while those in image C1 and C3 of Fig. 1 are smaller. At a biopolymer ratio of 1 w/v% BSA to 4 w/v% Ch, across all humidity values (Fig. 1, column D), again only protuberances were formed. Here the same general

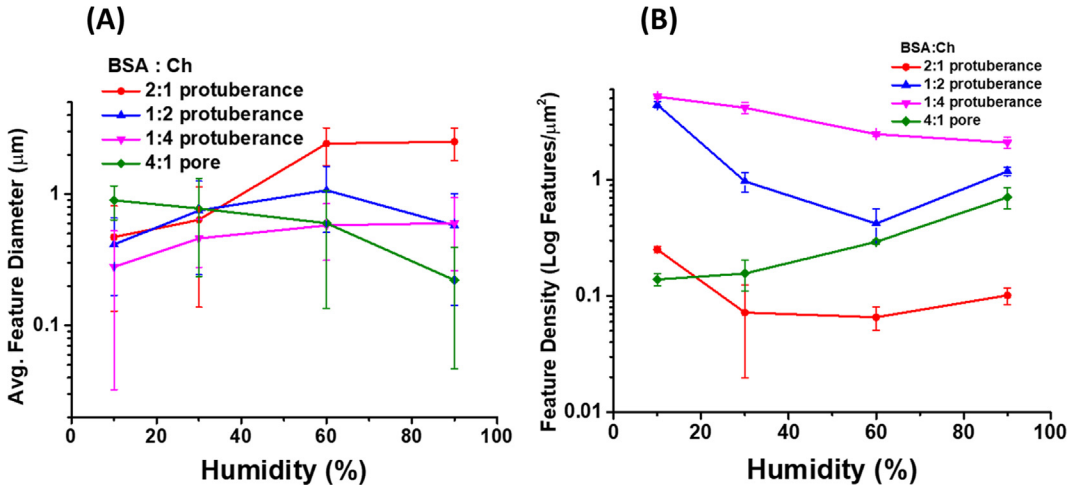

Fig. 2. Statistical analysis of BSA-Ch blends for feature size and density. All but the 4:1 blend refers to protuberance measurements, with the 4:1 blend data displaying pore data. (A) Refers to feature diameter plotted against humidity while (B) Details features/μm^2 vs.% humidity for 4:1, 2:1, 1:2 and 1:4 blends respectively.

trends outlined in column C were observed without deviations and attributed to a growth process, corroborated by AFM data analysis in Fig. 2a and b.

3.2.2. Thin-films from phase separation of PG-Ch-FA solutions

Fig. 3 shows a grid of AFM images of PG-Ch composite thin-films cast from PG-Ch-FA solutions. For these films, the features analysed by software were the protuberances as these were the features we were interested in controlling both the size and morphology of.

In thin films cast from a ratio of 4 w/v% PG to 1 w/v% Ch a wider variety of structures was seen than in the BSA-Ch films (Fig. 3, Column A). In films cast at 10% humidity protuberances were approx. 230 nm wide. Increasing humidity to 30% resulted in larger, but less defined protuberances (Fig. 3, panel A2).

Image A3 in Fig. 3 shows that 60% humidity yields poorly defined protuberances accompanied by pores. At 90% humidity, shown in image A4, ill-defined protuberances are observed on a much larger scale compared to the well-defined protuberances of image C1 and D3.

Fig. 4a and b show AFM data from PG-Ch blends highlighting a trend of increasing protuberance size and decrease in number with humidity. As with the BSA-Ch films previously discussed, this is indicative of a growth process. The precise nature of the growth process is discussed below.

Films cast from 2 w/v% PG 1 w/v% Ch (Fig. 3, column B) show a similar trend to those cast from 4 w/v% PG to 1 w/v% Ch but with fewer interconnects between protuberances, defining the protuberances more sharply.

Films cast from 1 w/v% PG 2 w/v% Ch (Fig. 3, column C), show a visual deviation from the trends observed in columns A and B of Fig. 3. Image C1 exhibits the best defined and smallest structures of any of the samples produced in this study, with protuberances of approximately 180 nm in diameter.

Image C2 presents a deviation from the trends observed up to now, with a particulated structure. The mean protuberance diameter and features per area of Fig. 4 presents no deviation. Software analysis of image C2 identified protuberance structures of a mean diameter larger than those in image C1 and smaller than those in image C3. However, inspection of these images with the naked eye clearly shows that a particulate morphology is formed. According to Doublier et al., thin-film microstructures formed from protein/polysaccharide blends can result from two simultaneously occurring processes: phase separation and gelation [34]. De Jong et al. expanded on this, showing that the final kinetically arrested structure in such instances originates from a competition between these two processes [62]. During the late stages of phase separation for many protein/polysaccharide systems, viscoelasticity in either one or both of the phases builds up, leading to a final gelled state of at least one of the phases. The morphology of this final stage is determined by the ratio of the rates of gelation and phase separation [33]. This creates difficulties when describing the structures arising from such phase-separated systems [63]. When the gelation of both phases is fast, a macroscopic gel is obtained with a bicontinuous structure. When the gelation is slow, phase separation can proceed until the phase highest in viscosity breaks up into droplets [33]. However, under certain conditions if the gelation of just one phase is rapid, phase separation can be hindered, as is the case with a PG-Ch system. As soon as the gelled protein network is formed, the separation of the phases is minimised or prevented and the system is "frozen" in a state determined by the gelation of the PG phase [34]. This frozen state offers an explanation for the structures observed in images C2, (and D1 and D2) of Fig. 3. What specifically caused the relatively rapid gelation of the PG under these conditions remains unclear. Given the inherent complexity and sensitivity of such systems it could be any number of the system parameters or, uncontrollable interactions between them.

Images D1 and D2 shown in Fig. 3, column D, are notably different from their equivalents in the previous columns, with spherical protuberances. However, according to the data shown in Fig. 4a and Fig. 5b, the same trends in feature size and number are also observed. This is a result of the particulated structure as described for image C2. Image D3 in Fig. 3 shows the most sharply defined protuberances of all PG-Ch films. These were the second smallest features with clear definition (approx. 389 nm) observed in our study and are in stark contrast to the features seen for the other PG-Ch films of different biopolymer ratio at the same humidity values. The protuberances are sharper, smaller and greater in number, the culmination of a trend in this direction with increasing Ch content at this humidity. These same observations can be made of the protuberances/globules seen in image D4 in comparison to their equivalents in images A4, B4, and C4.

3.2.3. General trends in Pr-Ps-S solution thin-films

The AFM images shown in Fig. 1 highlight a trend in pore formation at high protein (BSA) concentration to protuberance formation at high polysaccharide (Ch) content. Moving down the columns,

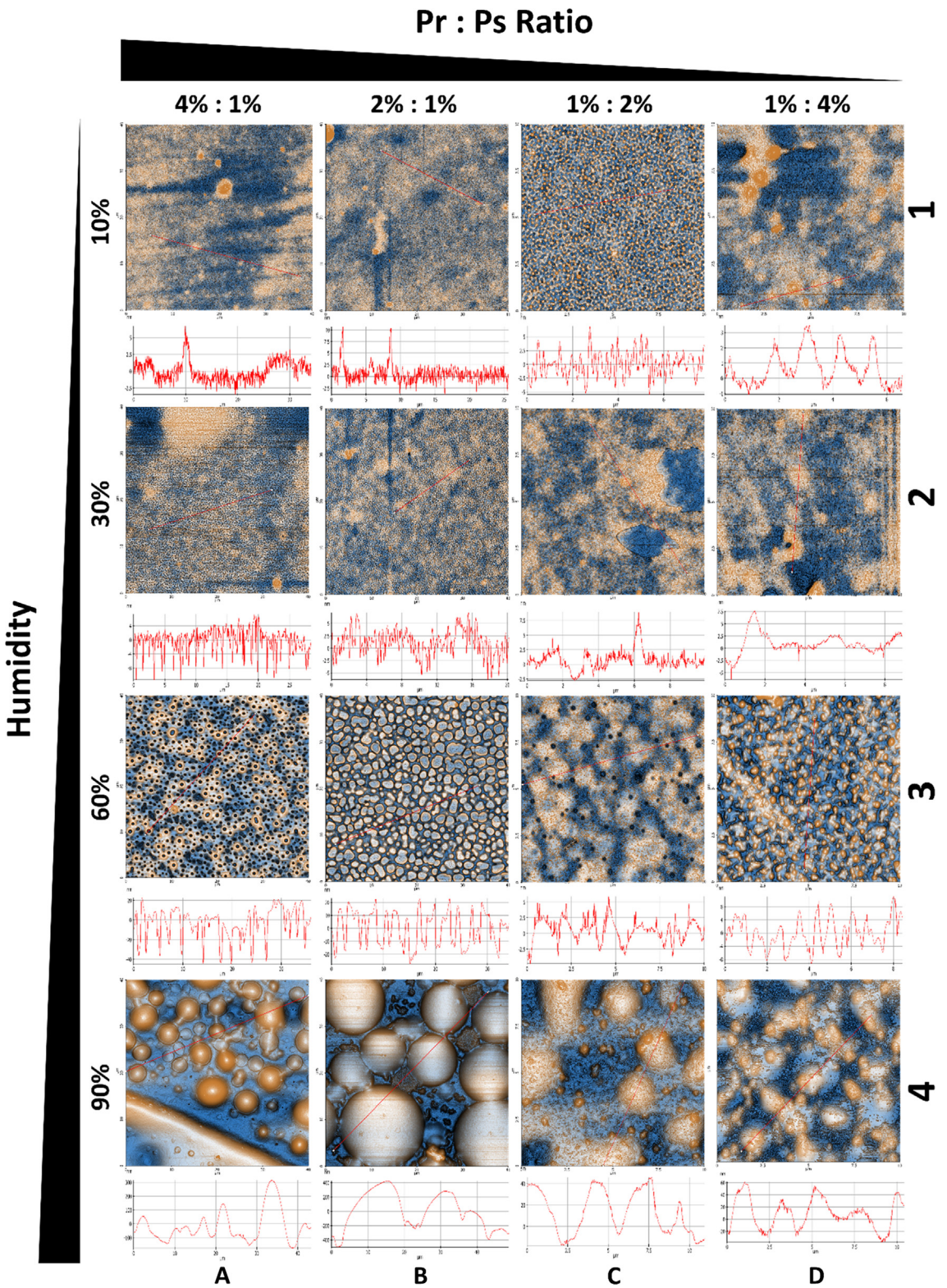

Fig. 3. AFM image grid and associated line profiles showing results of casting thin-films at 12 μm from specific Pr-Ps-S solutions of PG-Ch-FA at specific humidities. Each image in column A and column B is 40 μm × 40 μm area. Each image in column C and column D is 10 μm × 10 μm area. Column A = 4 w/v% PG 1 w/v% Ch (4:1), column B = 2 w/v% PG 1 w/v% Ch (2:1), column C = 1 w/v% PG 2 w/v% Ch (1:2), column D = 1 w/v% PG 4 w/v% Ch (1:4). Row 1 = 10% humidity, row 2 = 30% humidity, row 3 = 60% humidity and row 4 = 90% humidity.

changing humidity and maintaining the BSA:Ch ratio, there is a trend from smaller protuberance size at low humidity to larger protuberance size at high humidity; indicative of a protuberance growth process as humidity increases. Opposite trends are observed for the pores formed at the 4 w/v% BSA to 1 w/v% Ch ratio, suggesting they do not form by a growth process or, that pore growth is correlated with decreasing humidity. However, this is not the case for any other biopolymer ratios investigated.

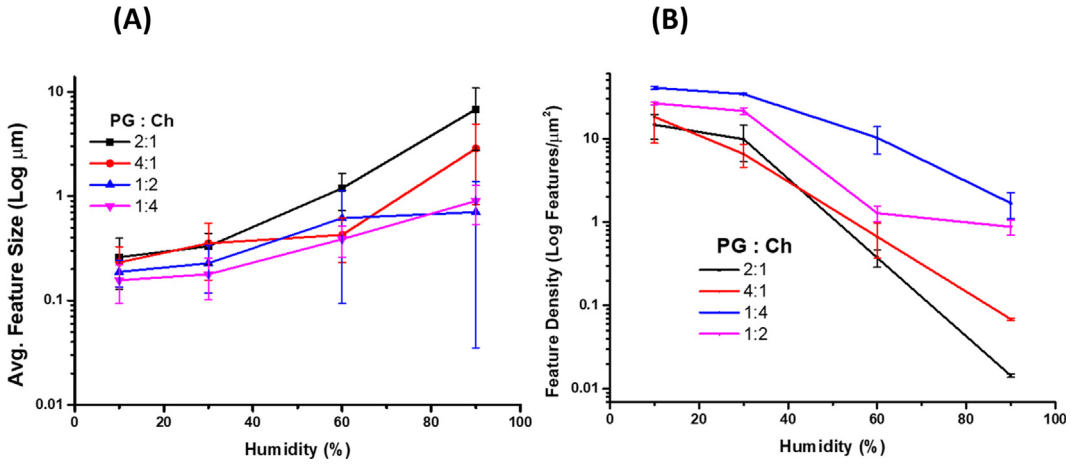

Fig. 4. Shows statistical analysis of PG-Ch blends for feature size and density. (A) Refers to feature diameter plotted against humidity. (B) Details features/μm^2 vs.% humidity.

Focusing on protuberances as the features conforming to a growth process behaviour, the images of PG-Ch blends from Fig. 3, as with BSA-Ch blends, show that increasing Ch concentration results in smaller protuberances. In addition, as with BSA-Ch, an increase in humidity leads to larger protuberances. Larger BSA-Ch protuberances appeared better defined than larger PG-Ch protuberances.

The root-mean-squared (RMS) roughness vs % humidity graphs in Fig. 5 showed similar trends increased protuberance diameter with increased humidity. All blends displayed increased roughness with increased humidity, similar to that of feature size. Slopes of 4:1 compared to 2:1, while 1:2 and 1:4 were similar with one another, except for the 2:1 BSA:Ch blend, which formed the tallest features at 60% humidity. RMS roughness is an indicator for applicability of materials to hydrophobic applications. In recent years, there has been much interest in developing rough high aspect ratio micro- and nanostructured surfaces to emulate the properties of self-cleaning and hydrophobic leaves [28,64,65].

Trommer et al. [28] have shown how certain mechanisms during demixing of incompatible polymer blends leads to the growth of large spherical structures in thin-films. These structures are similar to those seen throughout the images of Fig. 1 and Fig. 3. Size of spherical protuberances was controlled through polymer ratio and solution temperature [28]. Increased temperatures led to more extensive nucleation, due to the reduced viscosity of the solutions and higher polymer mobility, which resulted ultimately in larger structures. However, higher temperatures also resulted in faster rates of solvent evaporation. This loss of solvent increased solution viscosity, reducing polymer mobility, and so reducing the size of the spherical structures.

Although temperature was not varied for the Pr-Ps blends investigated in this study, similar structural growth trends were observed. AFM data shown in Figs. 2 and 4 revealed that humidity was the predominant factor for protuberance diameter. Drying time was proportional to relative humidity within the chamber. Low humidity permitted faster drying times while higher humidity provided longer drying times. As in the Trommer study [28] the greater rate of solvent loss increased solution viscosity, reducing polymer mobility, and so reducing the final size of the spherical structures. Such a growth process would explain the trends observed in the images of Fig. 1 and Fig. 3. Overall the AFM images of Fig. 1 and Fig. 3 seem to show the subsumption of smaller protuberances into larger ones with increased humidity. This is corroborated by the statistical data shown in Fig. 2 and Fig. 4, which highlights the increase in the mean protuberance size (approx. 7 μm) subsequent decrease in protuberance frequency for each blend with humidity; conforming to known growth processes, specifically, Ostwald ripening.

3.3. Feature growth in Pr-Ps-S thin-films

Ostwald ripening is a phase transition resulting from the coalescence of material. Ostwald ripening has been extensively studied in the formation of emulsions [66–68], controlling the size of crystals

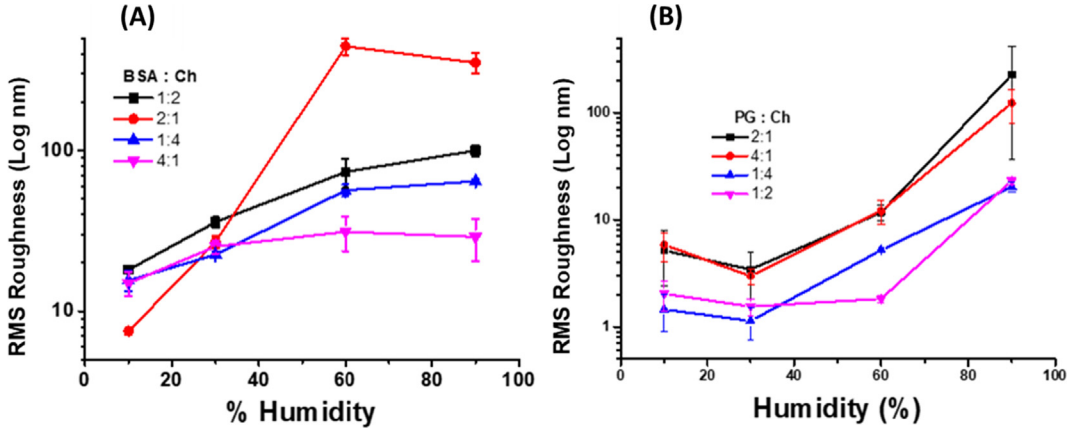

Fig. 5. Plots the RMS vs % humidity for all BSA-Ch blends. (B) Plots the RMS vs % humidity for all PG-Ch blends.

[69–71] and growing selective nanostructures [72–74]. The driving force of the process is a decrease in the total surface energy [75–77]. Characteristic trends in the evolution of cluster size distributions over time indicate Oswald ripening growth processes. In this instance, those characteristic trends were observed in the distribution and growth of spherical structures in the thin film surfaces. Unlike in materials where Oswald ripening is more commonly studied, annealing time was not a factor in the formation of the Pr-Ps thin films. Instead, relative humidity was controlled to limit the evaporation rate of formic acid [78]. As such, film drying rate and the length of time that the system has sufficient molecular mobility for growth to occur is controlled. Once the formic acid leaves the system, the biopolymer chains become locked in place. Thus, humidity in these experiments is proportional to time when observing Ostwald ripening.

The following observation was expected of a system undergoing Ostwald ripening; the counts per unit area (#) of protuberances would increase lower humidities while particle dimensions would decrease at low humidity due to high evaporation rate/insufficient time for growth phase. Furthermore, the opposite was expected to be observed at higher humidity values. This is precisely what was observed, with inset histograms required in Fig. 6b, Fig. 7a and b to show the expanded range at high humidity. Increased frequency of protuberances of smaller diameter are seen at low humidities. Conversely, fewer protuberances of greater diameter are observed at higher humidities.

Fig. 6 shows histogram data of feature diameter gathered for BSA-Ch blends. Fig. 6a displays the size distribution of the pores (predominant feature) in a 4:1 blend. As shown in the mean feature diameter size and humidity graphs, there is a shift towards smaller sizes with increased humidity. Fig. 6b–d display the size distributions of protuberances in the films. There is an increased frequency of protuberances of smaller diameter at low humidities, parallel to increased feature density. This effect is attributed to viscous Ch solutions reducing BSA polymer mobility, retarding the growth process. The frequency of larger protuberances increases with increased humidity and may be attributed to the formation of larger structures with longer drying times; suggesting that the growth mechanism occurs similarly to that of Ostwald ripening, as discussed earlier, with the consumption of smaller particles to form fewer larger particles.

Ostwald ripening in thin films follows a sinusoidal curve, so 2:1 may be closer to the midpoint. The 4:1 closely mirrors 1:2, again due to increasing number of holes preceding to the development of hills, and perhaps indicating that hole formation follows an inverse Ostwald ripening process.

Fig. 7 shows histogram data gathered for PG-Ch blends. A to D display the size distribution of protuberances in the film. Going from A to D results in an increased frequency of smaller protuberances at lower humidities, parallel to the increase in feature density. Again, this effect is attributed to viscous Ch solutions reducing PG polymer mobility, retarding the growth process. Frequency of protuberance numbers also reduced with increased humidity.

Histograms were normalised on the y axis for clarity. Data shows that for protuberance forming blends, a Gaussian population of protuberances was observed. For the 1:2 PG:Ch blend, it was possible to overlay Gaussian plots for 10%, 30%, 60% and 90%, showing the formation of larger features at higher humidities (see Figure 4 in Supporting Information). Phase imaging and the

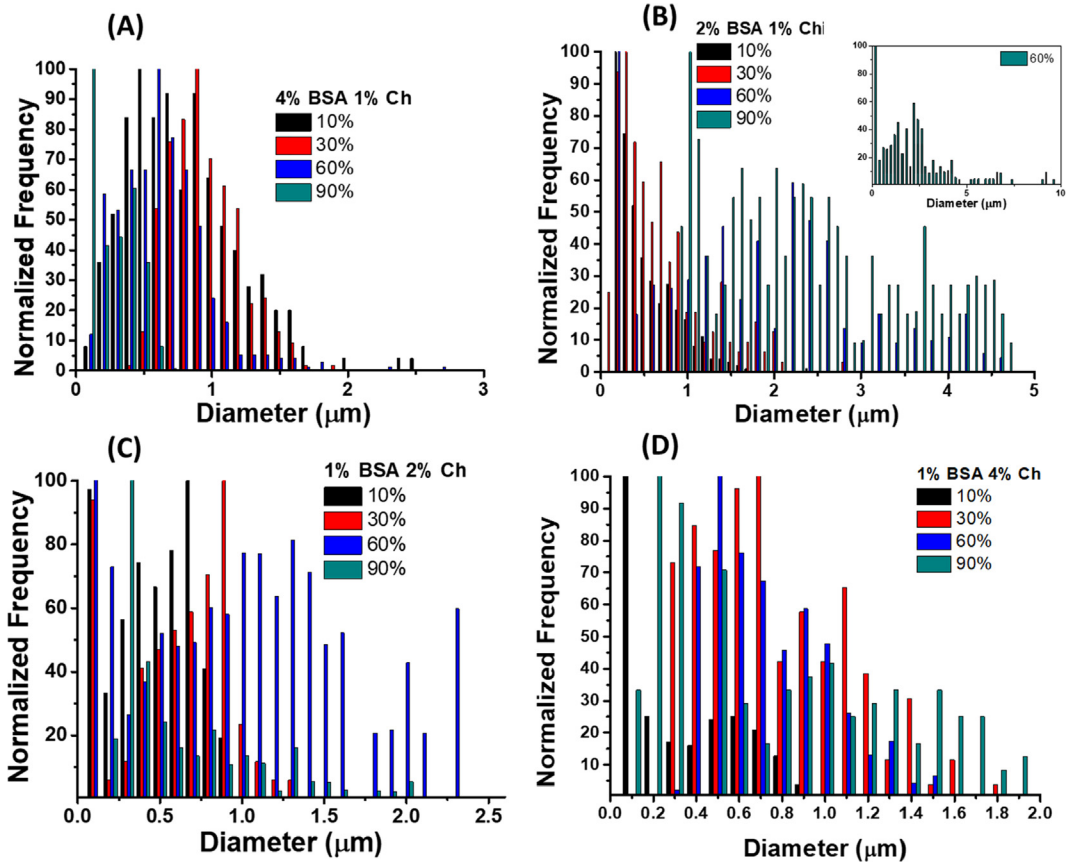

Fig. 6. Statistical analysis of BSA-Ch blends for feature and frequency of feature sizes. All but the 4:1 blend refers to protuberance measurements, with the 4:1 blend data displaying pore data. (A–D) displays feature count vs diameter of observed features for 4:1, 2:1, 1:2 and 1:4 blends respectively.

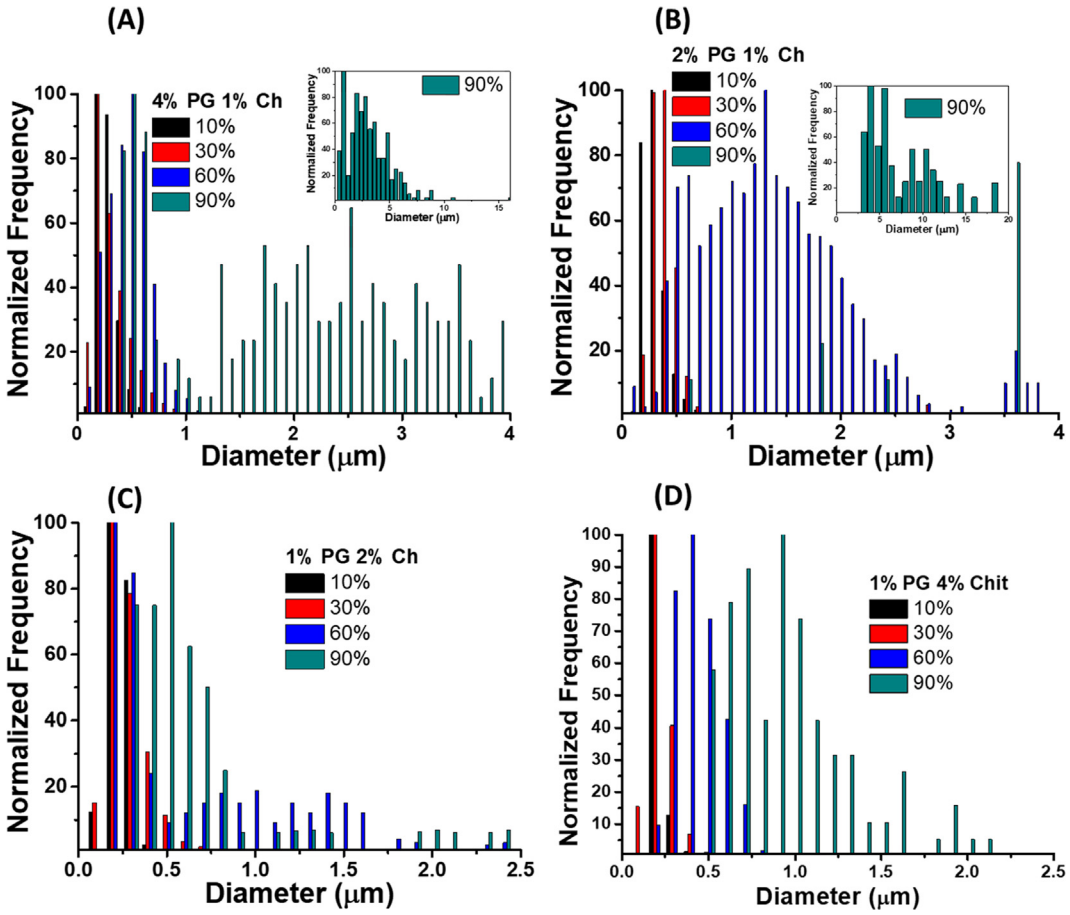

Fig. 7. Statistical analysis of PG-Ch blends for feature size and frequency of feature sizes. (A–D) displays feature count vs diameter of observed features for 4:1, 2:1, 1:2 and 1:4 blends respectively.

Young's modulus of both blends show protuberances (discontinuous domains) are composed of different a material to the underlying matrix (see Figure 5 and Figure 6 in Supporting Information). The 4:1 BSA:Ch plot shows the opposite, as in previous graphs, shifting towards smaller, more numerous holes consistent with other observations. They show the shift from a small number of large features to a large number of small features.

Fig. 5 displays RMS roughness of biopolymer blend films. There is an increase in the RMS roughness, parallel to the increase in feature size with increased humidity.

These results show it is possible to achieve sub-micron features utilizing only biologically sourced polymers. A particularly attractive property of biopolymer blends includes their self-assembly upon deposition and solvent evaporation, facilitating rapid pattern realisation and feature size tunability by easy control of the evaporation rate upon casting. This technique avoids the use of solvent annealing, functionalisation and pH control, while achieving the smallest domain size of such films to date. The combination of a viscous polysaccharide, volatile solvent and low humidity resulted in the first sub-micron structures obtained with a biopolymer blend seen in the literature. This could be further enhanced by choosing a higher molecular weight (M_w) chitosan. The increased viscosity due to the higher M_w would impede Ostwald ripening, resulting in smaller features of uniform spacing due to inhibited polymer mobility. A similar effect would be observed with a more viscous protein. Furthermore, other casting methods such as spin coating would achieve smaller feature sizes due to the faster rate of solvent removal, and would be further enhanced by humidity control. Reducing the overall concentration of the phase system could optimize domain spacing, size and definition. This would result in smaller features by reducing the amount of material available to feed into the discontinuous domain, and reduce the number of aggregated features on the surface, resulting in uniform monodispersed features. However, this method would likely result in conflicting mechanisms due to a reduction in overall viscosity of the system, promoting discontinuous domain growth. Finally, as with Trommer et al.'s work [28], temperature control could be employed in conjunction with this humidity regulated approach to achieve highly tuneable structures which would allow greater control over the materials properties and avoid functionalisation of components to improve domain definition. Such improvements would be required for applications in patterning and textiles.

4. Conclusion

This work has demonstrated that humidity is the defining factor in determining feature morphology and size in biopolymer blends, exceeding previously attained feature sizes in a facile and benign manner [28,30–32,35,62]. Segregative phase separation is successfully employed to achieve sub-micron structures. The use of a viscous polysaccharide, thin, wet deposit and low humidity in the casting process achieved a feature size of approx. 200 nm. Formic acid serves as a proficient solvent for most biopolymers, ensuring segregative phase separation and fast evaporation rates. The smallest feature sizes of both blends were achieved at 10% humidity with a high proportion of Ch in the casting blend. Protuberances observed in our films generally displayed higher monodispersity

at lower humidities and at higher Ch contribution, indicating this is caused by an impeded growth process. BSA blends produced well-defined large structures while PG blends produced well-defined small structures. The increased viscosity of PG solutions explains the smaller feature sizes in PG blends. Blend films display a similar growth mechanism regardless of category (high protein or high polysaccharide concentration); Ostwald ripening. The growth processes could be controlled more effectively with this insight. Our results show the smallest and most monodisperse features yet seen in such biopolymer films. However, the insights we have gained into the growth processes permit even smaller and more monodisperse feature size than those shown here, subject to effective controls. Due to the chemical properties of these blends, it is hoped that they will be employed as a cheaper and greener templating alternative. Such shifts in materials design are paramount in the progression towards a more sustainable future.

5. Supporting information available

3D topographical images, AFM images of neat biopolymer films and superimposed Gaussian profile of BSA-Ch blend are available in the Supporting Information.

Acknowledgements

Dr. Joseph Tobin of Glantreo Ltd., Ireland, Dr. John O'Connell of the Materials Chemistry and Analysis Group, University College Cork, Cork, Ireland. The Irish Research Council for Science, Engineering and Technology is also acknowledged for financial support of the work.

References

[1] F. Ferrarese Lupi, et al., High aspect ratio PS- *b* -PMMA block copolymer masks for lithographic applications, ACS Appl. Mater. Interfaces 6 (2014) 21389–21396.
[2] E. Sardella, P. Favia, R. Gristina, M. Nardulli, R. d'Agostino, Plasma-aided micro- and nanopatterning processes for biomedical applications, Plasma Process. Polym. 3 (2006) 456–469.
[3] F. Ouhib et al., Transparent superhydrophobic coatings from amphiphilic-fluorinated block copolymers synthesized by aqueous polymerization-induced self-assembly, Polym. Chem. 7 (2016) 3998–4003.
[4] J. Gao, X. Li, B. Li, Y. Han, Fabrication of polymer antireflective coatings by self-assembly of supramolecular block copolymer, Polymer 51 (2010) 2683–2689.
[5] S. Guldin, Inorganic Nanoarchitectures by Organic Self-Assembly, Springer International Publishing, 2013, pp. 141–154.
[6] T. van Vliet, in Food Macromolecules and Colloids 447–455, The Royal Society of Chemistry, 1995.
[7] P. Wilde, A. Mackie, F. Husband, P. Gunning, V. Morris, Proteins and emulsifiers at liquid interfaces, Adv. Colloid Interface Sci. 108–109 (2004) 63–71.
[8] Y. Matsushita, Microphase Separation (of Block Copolymers), Encyclopedia of Polymeric Nanomaterials, 2015, pp. 1255–1260.
[9] C. Chassenieux, D. Durand, P. Jyotishkumar, S. Thomas, in Handbook of Biopolymer-Based Materials: From Blends and Composites to Gels and Complex Networks 1–6, Wiley-VCH Verlag GmbH & Co KGaA, 2013.
[10] X.Z. Tang, P. Kumar, S. Alavi, K.P. Sandeep, Recent advances in biopolymers and biopolymer-based nanocomposites for food packaging materials, Crit. Rev. Food Sci. Nutr. 52 (2012) 426–442.
[11] R.L. Whistler, Carbohydrates in Solution, American Chemical Society, 1971, pp. 242–255.
[12] A.M. Striegel, J.D. Timpa, Molecular characterization of polysaccharides dissolved in Me2NAc-LiC1 by gel-permeation chromatography, Carbohydr. Res. 267 (1995) 271–290.
[13] G.D. Jovanović, A.S. Klaus, M.P. Nikšić, Antimicrobial activity of chitosan coatings and films against Listeria monocytogenes on black radish, Rev. Argent. Microbiol. 48 (2016) 128–136.
[14] J. Sun, H. Tan, Alginate-based biomaterials for regenerative medicine applications, Materials (Basel) 6 (2013) 1285–1309.
[15] Z. Saavedra-Leos, C. Leyva-Porras, S. Araujo-Díaz, A. Toxqui-Terán, A. Borrás-Enríquez, Technological application of maltodextrins according to the degree of polymerization, Molecules 20 (2015) 21067–21081.
[16] H. Cheng et al., Structural characterization and antioxidant activities of polysaccharides extracted from Epimedium acuminatum, Carbohydr. Polym. 92 (2013) 63–68.
[17] V. Tolstoguzov, Texturising by phase separation, Biotechnol. Adv. 24 (2006) 626–628.
[18] K. Sakamoto, R.Y. Lochhead, H.I. Maibach, Y. Yamashita, Cosmetic Science and Technology: Theoretical Principles and Applications, Elsevier, 2017.
[19] J.-H. Zhao, J. Wang, M. Tu, B.-H. Luo, C.-R. Zhou, Improving the cell affinity of a poly(D, L-lactide) film modified by grafting collagen via a plasma technique, Biomed. Mater. 1 (2006) 247–252.
[20] S. Petrulyte, Advanced textile materials and biopolymers in wound management, Dan. Med. Bull. 55 (2008) 72–77.
[21] W.N.R. Jami'an, et al., Effect of evaporation time on cellulose acetate membrane for gas separation, IOP Conf. Ser. Earth Environ. Sci. 36 (2016) 12008.
[22] A.R. Moghadassi, Z. Rajabi, S.M. Hosseini, M. Mohammadi, Fabrication and modification of cellulose acetate based mixed matrix membrane: gas separation and physical properties, J. Ind. Eng. Chem. 20 (2014) 1050–1060.
[23] S.A. Rahman, A.F. Ismail, W.A.W. Rahman, Formation of cellulose acetate membrane for gas separation from binary dope system: effect of shear rate, in: Proc. Reg. Symp. Membr. Sci. Technol., 2004, pp. 21–25.
[24] L.M. Robeson, Polymer blends in membrane transport processes, Ind. Eng. Chem. Res. 49 (2010) 11859–11865.
[25] M. Tallawi et al., Strategies for the chemical and biological functionalization of scaffolds for cardiac tissue engineering: a review, J. R. Soc. Interface 12 (2015) 20150254.
[26] X. Hu et al., The influence of elasticity and surface roughness on myogenic and osteogenic-differentiation of cells on silk-elastin biomaterials, Biomaterials 32 (2011) 8979–8989.
[27] S. Dörr, S. Hofacker, S. Viala, 'Hair setting composition' U.S. Patent Application 2010/0215608, 2010.
[28] K. Trommer, B. Morgenstern, F. Gähr, F. Hermanutz, Sub-micrometer structure textile coatings generated from cellulose based polymer blend, Lenzinger Berichte 87 (2009) 151–161.
[29] M. Yao et al., Microencapsulation of Lactobacillus salivarious Li01 for enhanced storage viability and targeted delivery to gut microbiota, Food Hydrocoll. 72 (2017) 228–236.
[30] I.C. Hoeger et al., Bicomponent lignocellulose thin films to study the role of surface lignin in cellulolytic reactions, Biomacromolecules 13 (2012) 3228–3240.
[31] S. Strasser et al., Exploring nonspecific protein adsorption on lignocellulosic amphiphilic bicomponent films, Biomacromolecules 17 (2016) 1083–1092.
[32] A. Peer, R. Dhakal, R. Biswas, J. Kim, Nanoscale patterning of biopolymers for functional biosurfaces and controlled drug release, Nanoscale 8 (2016).
[33] F. van de Velde, E.H.A. de Hoog, A. Oosterveld, R.H. Tromp, Protein-polysaccharide interactions to alter texture, Annu. Rev. Food Sci. Technol. 6 (2013) 371–388.
[34] J. Doublier, C. Garnier, D. Renard, C. Sanchez, Protein-polysaccharide interactions, Curr. Opin. Colloid Interface Sci. 5 (2000) 202–214.
[35] S. de Jong, F. van de Velde, Charge density of polysaccharide controls microstructure and large deformation properties of mixed gels, Food Hydrocoll. 21 (2007) 1172–1187.
[36] R.H. Tromp, E.H.A. De Hoog, Band formation on shearing in phase-separated polymer solutions, Phys. Rev. E - Stat. Nonlinear, Soft Matter Phys. 77 (2008) 1–7.
[37] J. Vermant, M.J. Solomon, Flow-induced structure in colloidal suspensions, J. Phys. Condens. Matter 17 (2005) R187–R216.
[38] Y. Yip, A.J. Mchugh, Modeling and simulation of nonsolvent vapor-induced phase separation, J. Memb. Sci. 271 (2006) 163–176.
[39] S. Tripathi, G.K. Mehrotra, P.K. Dutta, Chitosan based antimicrobial films for food packaging applications, e-Polymers 8 (2008) 93.
[40] Compatibilization in bio-based and biodegradable polymer blends, Eur. Polym. J. 49 (2013) 1215–1233.
[41] A.N. Nesmeyanov, E.V. Kikxadze, Concentration of proteins as a result of the phase separation of water-protein-polysaccharide systems Part 1. Phase equilibria in water-milk proteins-plysaccharide systems, Nahrung 30 (1986) 591–599.
[42] A.N. Nesmeyanov, N.A. Zhuravskaya, E.V. Kiknadze, V.B. Tolstoguzov, Concentration of proteins as a result of the phase separation of water-protein-polysaccharide systems Part 2 Concentration of milk proteins, Nahrung 30 (1986) 601–613.
[43] Y. Fang, L. Li, C. Inoue, L. Lundin, I. Appelqvist, Associative and segregative phase separations of gelatin/κ- carrageenan aqueous mixtures, Langmuir 22 (2006) 9532–9537.
[44] J.Y. Chun et al., Study of the phase separation behaviour of native or preheated WPI with polysaccharides, Polymer 55 (2014) 4379–4384.
[45] G.Q. Huang, Y.T. Sun, J.X. Xiao, J. Yang, Complex coacervation of soybean protein isolate and chitosan, Food Chem. 135 (2012) 534–539.
[46] Y. Yuan, Z.L. Wan, X.Q. Yang, S.W. Yin, Associative interactions between chitosan and soy protein fractions: effects of pH, mixing ratio, heat treatment and ionic strength, Food Res. Int. 55 (2014) 207–214.
[47] C. Elmer, A.C. Karaca, N.H. Low, M.T. Nickerson, Complex coacervation in pea protein isolate-chitosan mixtures, Food Res. Int. 44 (2011) 1441–1446.
[48] H.J. Lee, B. Jung, Y.S. Kang, H. Lee, Phase separation of polymer casting solution by nonsolvent vapor, J. Memb. Sci. 245 (2004) 103–112.
[49] H. Sun, S. Liu, B. Ge, L. Xing, H. Chen, Cellulose nitrate membrane formation via phase separation induced by penetration of nonsolvent from vapor phase, J. Memb. Sci. 295 (2007) 2–10.
[50] P Van Witte, Berg De, J.W.A. Van Den, J. Feijen, Phase separation processes in polymer solutions in relation to membrane formation, J. Memb. Sci. 117 (1996) 1–31.

[51] E.J. Flynn, J. Arndt, L. Brothier, M.A. Morris, Control of pore structure formation in cellulose nitrate polymer membranes, Adv. Chem. Sci. 2 (2013) 9–18.
[52] S.A. Idris, C. Robertson, M.A. Morris, L.T. Gibson, A comparative study of selected sorbents for sampling of aromatic VOCs from indoor air, Anal. Methods 2 (2010) 1803.
[53] Japanese-Standards-Association. Geometrical Product Specifications (GPS) – Surface texture: profile method – Terms, definitions and surface texture parameters, Japanese Ind. Stand. B 601 (2013).
[54] Japanese-Standards-Association. Geometrical Product Specifications (GPS) - Indication of surface texture in technical product documentation, Japanese Ind. Stand. B 31 (2003).
[55] Y.-S. Kang, H.-J. Kim, Y.-H. Kim, W.-H. Jo, The mechanism of assymetric membrane formation via phase inversion, Polym. Soc. Korea 12 (1988) 279–287.
[56] H. Chae Park, Y. Po Kim, H. Yong Kim, Y. Soo Kang, Membrane formation by water vapor induced phase inversion, J. Memb. Sci. 156 (1999) 169–178.
[57] M.N.V.R. Kumar, A review of chitin and chitosan applications, React. Funct. Polym. 46 (2000) 1–27.
[58] C.K.S. Pillai, W. Paul, C.P. Sharma, Chitin and chitosan polymers: chemistry, solubility and fiber formation, Prog. Polym. Sci. 34 (2009) 641–678.
[59] G. Houen, The solubility of proteins in organic solvents, Acta Chem. Scand. 50 (1996) 68–70.
[60] D.J. Shaw, Introduction to Colloid and Surface Chemistry, Butterworth - Heinemann, 1992, pp. 1–10.
[61] K.J. Laidler, J.H. Meiser, B.C. Sanctuary, Physical Chemistry, Houghton Mifflin Company, 2003, pp. 929–965.
[62] S. de Jong, H.J. Klok, F. van de Velde, The mechanism behind microstructure formation in mixed whey protein-polysaccharide cold-set gels, Food Hydrocoll. 23 (2009) 755–764.
[63] D.V. Zasypkin, E.E. Braudo, V.B. Tolstoguzov, Multicomponent biopolymer gels, Food Hydrocoll. 11 (1997) 159–170.
[64] C. Yang, U. Tartaglino, B.N.J. Persson, Influence of surface roughness on superhydrophobicity, Phys. Rev. Lett. 97 (2006) 116103.
[65] H.J. Ensikat, P. Ditsche-Kuru, C. Neinhuis, W. Barthlott, Superhydrophobicity in perfection: the outstanding properties of the lotus leaf, Beilstein J. Nanotechnol. 2 (2011) 152–161.
[66] F.M.J. Mirabella, J.S. Barley, Ostwald ripening in lmmiscible polyolefin blends, J. Polym. Sci. Pol. Phys. 33 (1995) 2281–2287.
[67] T.J. Wooster, M. Golding, P. Sanguansri, Impact of oil type on nanoemulsion formation and ostwald ripening stability, Langmuir 24 (2008) 12758–12765.
[68] A. Gupta, H.B. Eral, T.A. Hatton, P.S. Doyle, Nanoemulsions: formation, properties and applications, Soft Matter 12 (2016) 2826–2841.
[69] A. Baldan, Review Progress in Ostwald ripening theories and their applications to the γ′-precipitates in nickel-base superalloys Part II Nickel-base superalloys, J. Mater. Sci. 37 (2002) 2379–2405.
[70] W. Zhu et al., Coarsening of one-step deposited organolead triiodide perovskite films via Ostwald ripening for high efficiency planar-heterojunction solar cells, Dalt. Trans. 45 (2016) 7856–7865.
[71] M. Yang et al., Facile fabrication of large-grain CH3NH3PbI3-xBrx films for high-efficiency solar cells via CH3NH3Br-selective Ostwald ripening, Nat. Commun. 7 (2016) 2–10.
[72] M. Oliva-Ramirez, M. Macías-Montero, A. Borras, A.R. González-Elipe, Ripening and recrystallization of NaCl nanocrystals in humid conditions, RSC Adv. 6 (2016) 3778–3782.
[73] O. Lotty et al., Self-seeded growth of germanium nanowires: coalescence and Ostwald ripening, Chem. Mater. 25 (2013) 215–222.
[74] A. Imre, E. Gontier-Moya, D.L. Beke, I.A. Szabó, G. Erdélyi, Ostwald ripening of Pd particles on the (10 1 2) surface of sapphire, Surf. Sci. 441 (1999) 133–139.
[75] K.B. Glasner, Ostwald ripening in thin film equations, SIAM J. Appl. Math. 69 (2008) 473–493.
[76] S. Dai, On the Ostwald ripening of thin liquid films, Commun. Math. Sci. 9 (2011) 143–160.
[77] G. Madras, B.J. McCoy, Ostwald ripening in two dimensions: time dependence of size distributions for thin-film islands, Phys. Chem. Chem. Phys. 5 (2003) 5459.
[78] D. Mackay, I. Van Wesenbeeck, Correlation of chemical evaporation rate with vapor pressure, Environ. Sci. Technol. 48 (2014) 10259–10263.